ARTICLE

doi:10.1038/nature14561

Competitive binding of antagonistic peptides fine-tunes stomatal patterning

Jin Suk Lee[1,2], Marketa Hnilova[3], Michal Maes[2], Ya-Chen Lisa Lin[1,2], Aarthi Putarjunan[2], Soon-Ki Han[1,2], Julian Avila[1,2] & Keiko U. Torii[1,2]

During development, cells interpret complex and often conflicting signals to make optimal decisions. Plant stomata, the cellular interface between a plant and the atmosphere, develop according to positional cues, which include a family of secreted peptides called epidermal patterning factors (EPFs). How these signalling peptides orchestrate pattern formation at a molecular level remains unclear. Here we report in *Arabidopsis* that Stomagen (also called EPF-LIKE9) peptide, which promotes stomatal development, requires ERECTA (ER)-family receptor kinases and interferes with the inhibition of stomatal development by the EPIDERMAL PATTERNING FACTOR 2 (EPF2)-ER module. Both EPF2 and Stomagen directly bind to ER and its co-receptor TOO MANY MOUTHS. Stomagen peptide competitively replaced EPF2 binding to ER. Furthermore, application of EPF2, but not Stomagen, elicited rapid phosphorylation of downstream signalling components *in vivo*. Our findings demonstrate how a plant receptor agonist and antagonist define inhibitory and inductive cues to fine-tune tissue patterning on the plant epidermis.

Development and pattern formation of multicellular organisms rely on diffusible signals that instruct cells to adopt a specific fate for optimal function, and hence organismal fitness. Often such signals are encoded by multiple gene families, which raises the question of how a given cell orchestrates the decision-making process. For instance, a family of secreted signals, such as FGFs, are used in an iterative manner to specify multiple, diverse developmental processes in animals[1]. While peptide signalling has recently emerged as a critical regulator of plant development[2], how specific members of plant peptide families share and distribute functions remains unclear. Patterning of stomata—valves on the plant epidermis that mediate carbon dioxide acquisition and water control—relies on cell–cell communication, which specifies a subset of seemingly uniform protodermal cells to acquire stomatal progenitor fate. Two secreted cysteine-rich peptides, EPF1 and EPF2, are expressed in later and earlier stages of stomatal precursors, respectively, and are perceived by the cell-surface receptors, ER-family leucine-rich repeat receptor kinases (LRR-RKs)—ER, ER-LIKE1 (ERL1) and ERL2—to inhibit stomatal development[3–7]. The receptor-like protein TOO MANY MOUTHS (TMM) modulates the signalling strengths of ER-family receptor kinases in a region-specific manner[6,8]. Genetic evidence suggests that the signals are mediated via a mitogen-activated protein kinase (MAPK) cascade, which eventually downregulates the transcription factor responsible for initiating stomatal lineage via direct phosphorylation[9–12].

Recently, EPF-LIKE9 (EPFL9) peptide, also known as Stomagen, was identified as a positive regulator of stomatal development, a role opposite to EPF1 and EPF2 (refs 13–17). Structural modelling of the EPF/EPFL-family peptides using the NMR-solved structure of Stomagen predicts that they all adopt related structures[16]. This raises the question of how can structurally related peptides confer completely opposite developmental responses. The molecular mechanism for Stomagen action remains unknown.

Stomagen acts downstream of the ER family

To place Stomagen into a genetic framework of the core stomatal signalling pathway, we first examined the effects of induced *STOMAGEN* overexpression (*iSTOMAGEN*) on *er erl1 erl2* triple mutant phenotypes by an oestradiol-induction system or co-suppression by artificial microRNA (*STOMAGEN-ami*) (Fig. 1 and Extended Data Figs 1–4). As previously reported[13,14], ectopic *iSTOMAGEN* expression resulted in an increase in stomatal density (number of stomata per mm^2), stomatal index (percentage of stomata per total number of stomatal and non-stomatal epidermal cells) and severe stomatal clustering in wild-type cotyledon epidermis (Fig. 1a, b, k and Extended Data Figs 1–3). In contrast, *iSTOMAGEN* had no effect on stomatal density, stomatal index, or stomatal clusters in *er erl1 erl2* cotyledons, just like in *tmm* (Fig. 1 and Extended Data Fig. 3)[13,14], suggesting that *STOMAGEN* and the *ER* family act in the same pathway.

As reported, *STOMAGEN-ami* lines markedly reduced stomatal development in wild-type cotyledons (Fig. 1a, c, j and Extended Data Fig. 4)[13]. In contrast, *STOMAGEN-ami* had no effect on stomatal density, stomatal index, and stomatal clustering phenotype of *er erl1 erl2* cotyledons, just like *tmm* (Fig. 1 and Extended Data Fig. 4). Thus, ER-family receptor kinases are required for the hypermorphic and hypomorphic effects of Stomagen. The epistasis of *er erl1 erl2* stomatal cluster phenotype over the phenotype of *STOMAGEN-ami* places the *ER* family downstream of *STOMAGEN*, consistent with the molecular identity of their gene products as receptor kinases and a secreted peptide.

Genetic dissection of Stomagen action

To dissect the role of Stomagen on the TMM and ER module, we comprehensively investigated the effects of *iSTOMAGEN* on stomatal differentiation in *tmm* hypocotyls with additional *er*-family mutations (Fig. 2 and Extended Data Fig. 5). In hypocotyls, *TMM* and *ER* family have opposite functions: *tmm* hypocotyls lack stomata[18], whereas *er erl1 erl2* hypocotyls produce stomatal clusters[19]. While *tmm* is epistatic to *er* single mutation in hypocotyls, consecutive loss of *ER*-family genes reverts stomatal development in a dosage-dependent manner, with *er erl1 erl2* being epistatic to *tmm* (ref. 7). *iSTOMAGEN* does not confer stomatal differentiation in *tmm*

[1]Howard Hughes Medical Institute, University of Washington, Seattle, Washington 98195, USA. [2]Department of Biology, University of Washington, Seattle, Washington 98195, USA. [3]Department of Materials Science and Engineering, University of Washington, Seattle, Washington 98195, USA.

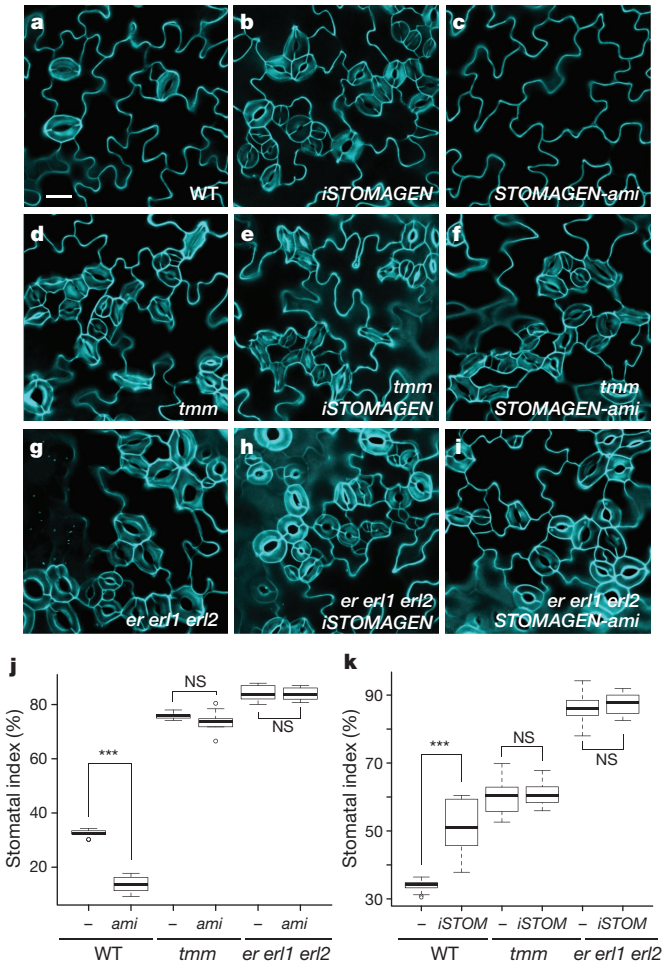

Figure 1 | Complete loss of *ER*-family genes confers insensitivity to *STOMAGEN* overexpression and co-suppression. **a**–**i**, Representative confocal images of cotyledon abaxial epidermis from 10-day-old light-grown seedlings of wild type (**a**–**c**), *tmm* (**d**–**f**) and *er erl1 erl2* (**g**–**i**), with induced *STOMAGEN* overexpression (*iSTOMAGEN*; **b**, **e**, **h**) or *STOMAGEN-ami* construct (**c**, **f**, **i**). Uninduced controls show no effects (see Extended Data Figs 1–3). Images were taken under the same magnification. Scale bar, 30 μm. $n = 13$ (**a**); $n = 18$ (**b**); $n = 26$ (**c**); $n = 16$ (**d**); $n = 24$ (**e**); $n = 26$ (**f**); $n = 16$ (**g**); $n = 24$ (**h**); $n = 12$ (**i**). **j**, Stomatal index. −, control; *ami*, *STOMAGEN-ami*. Box, mean; bars, s.e.m. $^{***}P < 0.005$ (Wilcoxon rank sum test). NS, not significant ($P = 0.653$ for *tmm*; $P = 0.539$ for *er erl1 erl2*). $n = 8$ for each genotype. **k**, Stomatal index. −, uninduced; *iSTOM*, induced. Box, mean; bars, s.e.m. $^{***}P < 0.005$ (Wilcoxon rank sum test). NS, not significant ($P = 0.114$ for *tmm*; $P = 0.688$ for *er erl1 erl2*). No induction, $n = 16$; *iSTOM*, $n = 14$; *tmm* no induction, *tmm iSTOM*, *er erl1 erl2*, *er erl1 erl2 iSTOM*, $n = 15$ for each genotype. For the total numbers of stomata counted, see legends for Extended Data Figs 3 and 4.

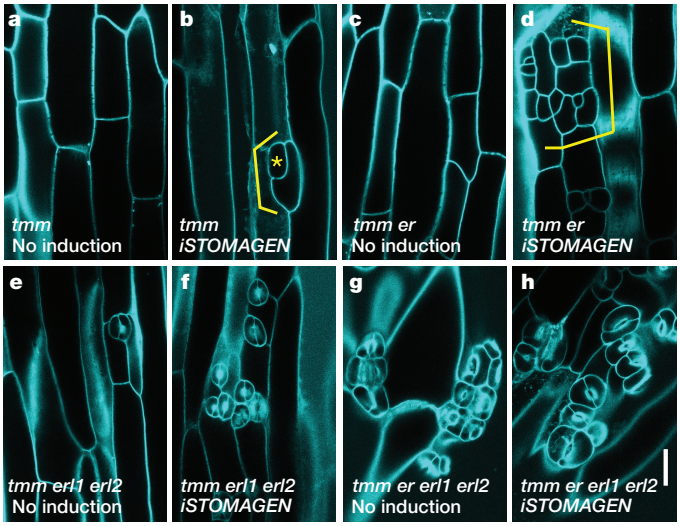

Figure 2 | *STOMAGEN* overexpression on stomatal development in *tmm* hypocotyl epidermis with combinatorial loss-of-function in *ER*-family genes. **a**–**h**, Representative confocal microscopy images of hypocotyl epidermis from 10-day-old light-grown transgenic *Est::STOMAGEN* (oestradiol-induced *STOMAGEN*) seedlings of *tmm* (**a**, **b**); *tmm er* (**c**, **d**); *tmm erl1 erl2* (**e**, **f**); and *tmm er erl1 erl2* (**g**, **h**). A control, uninduced phenotype (**a**, **c**, **e**, **g**) and *iSTOMAGEN* phenotype (**b**, **d**, **f**, **h**) is shown. *iSTOMAGEN* results in arrested stomatal precursor cells (asterisk) and stomatal-lineage ground cells (SLGCs (bracket)) in *tmm* hypocotyls (**b**). Additional *er* mutation exaggerated this effect (**d**), while additional *erl1 erl2* mutations increased stomata (**f**). Images were taken under the same magnification. Scale bar, 30 μm. $n = 20$ (**a**); $n = 20$ (**b**); $n = 19$ (**c**); $n = 22$ (**d**); $n = 17$ (**e**); $n = 20$ (**f**); $n = 20$ (**g**), $n = 20$ (**h**). For a complete set of higher-order mutant phenotypes and quantitative data, see Extended Data Fig. 5.

hypocotyls[13]. However, in some instances arrested stomatal precursor cells (stomatal-lineage ground cells (SLGCs)) were observed, indicating that, in the absence of *TMM*, *iSTOMAGEN* could initiate stomatal development in hypocotyls (Fig. 2a, b and Extended Data Fig. 5c, d). Additional *er*-family mutations exaggerated this effect; that is, *iSTOMAGEN* in *tmm er* and *tmm erl2* hypocotyls, both of which lack stomata, resulted in SLGC clusters (Fig. 2c, d and Extended Data Fig. 5e–h). *iSTOMAGEN* triggered stomatal cluster formation in *tmm erl1*, *tmm erl1 erl2* and *tmm er erl1* mutant hypocotyls, while intensifying stomatal entry divisions in *tmm er erl2* hypocotyls (Fig. 2e, f and Extended Data Fig. 5i–p). Different effects of *iSTOMAGEN* on the higher-order mutants lacking *ER* (for example, *tmm er* and *tmm er erl2*) compared with those lacking *ERL1* (for example, *tmm erl1* and *tmm erl1 erl2*) reflect the overlapping yet unique roles of *ER* and *ERL1* in stomatal development[6]. Finally, *iSTOMAGEN* failed to enhance the severe stomatal clustering phenotype in *tmm er erl1 erl2* mutants (Fig. 2g, h and Extended Data Fig. 5q, r). Quantitative analysis of stomatal index and SLGC index (the percentage of SLGCs in total epidermal cells) supports these findings (Extended Data Fig. 5s, t). Together, the results suggest that in the hypocotyls, where TMM and ER-family act antagonistically, Stomagen primarily acts via all three ER-family receptor kinases.

Among the ER family, ER primarily perceives EPF2 to restrict initiation of stomatal cell lineages, while ERL1 primarily perceives EPF1 to orient stomatal spacing and prevent guard cell differentiation[6]. As such, *epf2* increases SLGCs, whereas *epf1* violates stomatal spacing[3–5]. Neither *epf2* nor *epf1* confers severe stomatal clustering phenotype like *iSTOMAGEN*, since only a subset of *ER*-family-mediated pathways has been compromised[6]. We delineated the role of Stomagen in each of these steps. We first examined whether *EPF1*, *EPF2* and *STOMAGEN* transcripts are under feedback regulation, which may complicate the genetic analyses. *EPF1* and *EPF2* transcript levels were slightly upregulated by *iSTOMAGEN*, and conversely, slightly downregulated by *STOMAGEN-ami* (Extended Data Fig. 2c, d). However, the endogenous *STOMAGEN* transcript levels are unaffected by *epf1*, *epf2*, or *epf1 epf2* (Extended Data Fig. 2d). Thus, altered expression of *EPF1* and *EPF2* by *STOMAGEN* misregulation probably reflects the numbers of stomatal-lineage cells[13,14].

EPF2–ER or EPF1–ERL1 signalling pathways with *iSTOMAGEN* resulted in severe stomatal clusters, indicating that excessive Stomagen promotes stomatal differentiation when either pathway is compromised (Extended Data Fig. 3). These genetic data support the notion that Stomagen, when ectopically overexpressed, can bind to all ER-family receptor kinases and inhibit signal transduction. Indeed, co-immunoprecipitation experiments using *Nicotiana benthamiana* microsomal fraction expressing green fluorescent protein (GFP)-fused ectodomains of ER, ERL1, ERL2 or TMM incubated

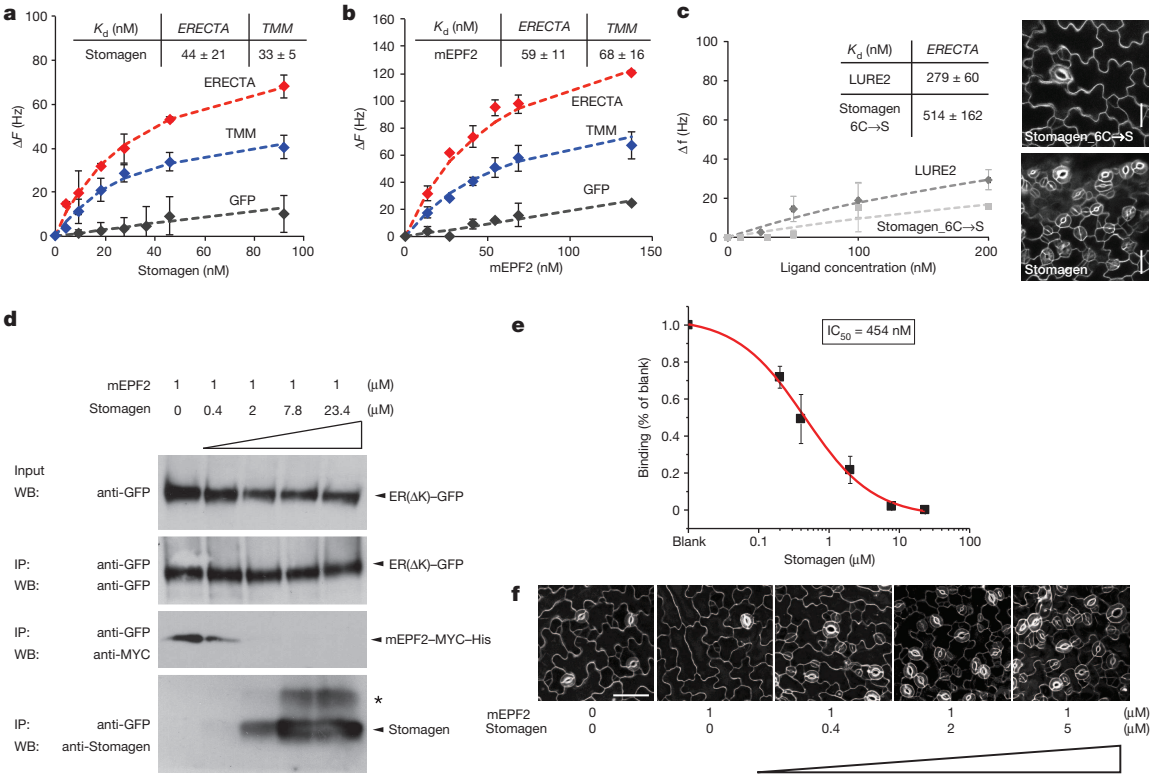

Figure 3 | Direct and competitive binding of Stomagen and EPF2 peptides to ER. **a**–**c**, QCM analysis for direct binding. **a**, **b**, The averages of experimental frequency shift values recorded from two to four independent experiments for Stomagen (**a**) or mEPF2 (**b**) onto biosensor chips functionalized with ER(ΔK)–GFP (red), TMM–GFP (blue) and GFP alone (grey) and fitted to the Langmuir adsorption model using least square regression. Error bars indicate s.d. Stomagen–ER, $n = 3$; Stomagen–TMM, $n = 2$; Stomagen–GFP, $n = 3$; mEPF2–ER, $n = 2$; mEPF2–TMM, $n = 3$; mEPF2–GFP, $n = 2$. **c**, The average experimental frequency shift values recorded for LURE2 (dark grey) and mutant Stomagen (light grey) on ER(ΔK)–GFP. To calculate the dissociation constant (K_d) values, the ligand concentrations were increased to 1 μM to obtain fitted curves. See Extended Data Fig. 9 for raw recording data. Inactive mutant Stomagen, in which six cysteines were substituted with serines (Stomagen_C6→S)–ER, $n = 3$; LURE2–ER, $n = 2$. Error bars indicate s.d. Right insets: wild-type cotyledon epidermis treated with 2.5 μM mutant or bioactive Stomagen. Scale bars, 30 μm. $n = 8$ for each treatment. For **a**–**c**, each experimental point in independent binding experiment (referred to as '$n = 1$') is generated from multi-point raw data (10–20 points) with average and s.d. values. **d**, Competitive binding. Microsomal fractions expressing ER(ΔK)–GFP were incubated with 1 μM of bioactive mEPF2 with increasing concentrations of bioactive Stomagen and subjected to immunoprecipitation. The mEPF2–MYC–His blot was re-probed with anti-Stomagen antibody. Asterisk indicates most likely isomer. **e**, Quantitative analysis of competition from four biological replicates. Error bars, s.e.m. The IC_{50} value is substantially higher than the K_d values for Stomagen–ER or mEPF2–ER, presumably owing to the immunoblot-based quantification. **f**, Wild-type cotyledon epidermis treated with mEPF2 alone or simultaneously co-treated with mEPF2 and increasing concentrations of Stomagen for 5 days. $n = 3$ for each treatment. Images were taken under the same magnification. Scale bar, 50 μM.

with synthetic Stomagen peptides demonstrated that Stomagen associates with all ER-family receptor kinases and TMM (Extended Data Fig. 6a).

Unlike overexpression, Stomagen co-suppression imposed different effects on EPF2–ER and EPF1–ERL1 signalling pathways. *STOMAGEN-ami* suppressed the stomatal-pairing phenotype of *epf1* and dominant-negative, kinases-deleted ERL1 (ERL1(ΔK)) *erl1* (Extended Data Fig. 4g–j, m). In contrast, *STOMAGEN-ami* exhibited complex interactions with *epf2* and dominant-negative ER (ER(ΔK)) *er,* reducing numbers of stomata but not that of SLGCs (Extended Data Fig. 4c–f, k–n). This supports the idea that Stomagen counteracts EPF2 for ER-mediated stomatal initiation[13,14,16]. This also suggests that, in the absence of both *EPF2* and *STOMAGEN*, the default ER pathway is not activated while the later ERL-mediated pathway remains capable of repressing the differentiation of mature stomata.

Competitive binding of EPF2 and Stomagen

A series of genetic analyses leads to the possibility that Stomagen antagonizes EPF2's action via direct binding to ER. To address this, we produced bioactive Stomagen and predicted mature EPF2 (mEPF2) peptides (Extended Data Figs 7 and 8). Subsequently, their direct binding to ER as well as to TMM was tested using previously established quartz crystal microbalance (QCM) biosensor platforms (Fig. 3a, b and Extended Data Fig. 9)[6]. Briefly, we immobilized purified GFP-fused receptors or control GFP from *N. benthamiana* on gold surfaces of QCM chips via anti-GFP antibody and then introduced the bioactive Stomagen or mEPF2 peptide solutions. The peptide–receptor binding was recorded as a function of frequency change (see Methods)[6]. Both Stomagen and mEPF2 exhibited saturable binding to the ER ectodomain fused to GFP (ER(ΔK)–GFP) with similar dissociation constants at a nanomolar range (Fig. 3a, b and Extended Data Fig. 9). Additionally, Stomagen and mEPF2 bound to TMM with high affinity (Fig. 3a, b). No significant binding of Stomagen or mEPF2 to control GFP was detected (Fig. 3a, b and Extended Data Fig. 9). To address the specificity of peptide–receptor interactions, two control peptides were subjected to the QCM analysis using ER(ΔK)–GFP-functionalized chips: (1) non-folding, inactive mutant Stomagen, in which six cysteines were substituted with serines (Extended Data Fig. 8g)[16]; and (2) LURE2, an unrelated cysteine-rich peptide, which acts as a pollen-tube attractant[20]. Neither mutant Stomagen nor LURE2 exhibited binding above the background level (Fig. 3c). Consistently, LURE2 did not associate with ER, TMM, or an innate immunity receptor FLS2 (refs 21, 22) fused with GFP expressed in *N. benthamiana* in co-immunoprecipitation assays (Extended Data

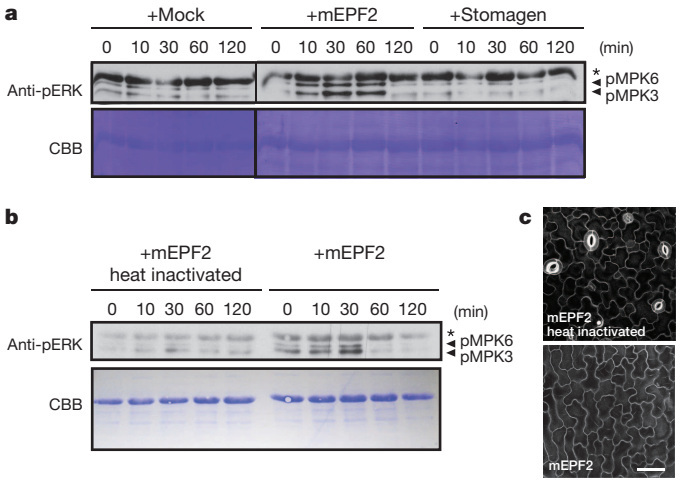

Figure 4 | EPF2, but not Stomagen, triggers downstream MAPK activation in *Arabidopsis* seedlings. **a**, **b**, Differential MAPK activation in *Arabidopsis* wild-type seedlings treated with buffer only (**a**, mock), mEPF2 (**a**, **b**), Stomagen (**a**), and heat-denatured mEPF2 (**b**) for respective time intervals (min). The blots were probed with anti-phospho-ERK antibody (anti-pERK) to detect phosphorylated MPK6 (pMPK6) and pMPK3 upon peptide treatment. Asterisk indicates non-specific band. CBB, total proteins stained. Four and two biological replicates were performed for **a** and **b**, respectively. **c**, Confocal microscopy of *Arabidopsis* wild-type cotyledon abaxial epidermis treated with heat-denatured mEPF2 (top) and control, non-denatured mEPF2 (bottom). Scale bar, 40 μm. $n = 3$ for each treatment.

Fig. 6b). Similarly, FLS2 failed to immunoprecipitate Stomagen above background levels (Extended Data Fig. 6c). Together, the results emphasize the specificity of Stomagen–ERECTA and Stomagen–TMM interactions.

Next, we performed ligand competition assays between Stomagen and EPF2. Microsomal fractions from *N. benthamiana* expressing ER ectodomain (ER(ΔK)–GFP) were incubated with bioactive epitope-tagged mEPF2 (mEPF2–MYC–HIS; 1 μM) and increasing concentrations of bioactive Stomagen peptides (0–23.4 μM) followed by immunoprecipitation of ER. Co-immunoprecipitated epitope-tagged mEPF2 was detected first. Then, the same blot was re-probed with anti-Stomagen antibody to detect co-immunoprecipitated Stomagen. Increasing concentrations of Stomagen peptide replaced mEPF2 for ER binding (Fig. 3d). Quantitative analysis confirmed the competitive binding of Stomagen and mEPF2 to ER, with a half-maximum inhibitory concentration (IC_{50}) value of 454 nM (Fig. 3e). Our results demonstrate that Stomagen and EPF2 peptides directly compete for binding to the same receptor, ER. Application of mEPF2 to wild-type seedlings inhibited stomatal development, while simultaneous treatment of mEPF2 with increasing concentration of Stomagen in a similar concentration range used in the competition experiments resulted in increased stomatal differentiation (Fig. 3f). The results are consistent with a previous report[16] and further emphasize the *in vivo* biological relevance of peptide competition.

Activation of downstream signalling

To unravel the mechanism of Stomagen as a competitive antagonist of EPF2, we examined the activation of downstream signalling, specifically, using phosphorylation of MPK3 and MPK6 as readout. Genetic studies suggest that EPF2–ER ligand–receptor signalling acts via a MAPK cascade[9–12]. However, a recent report of co-expressed stomatal signalling components in *N. benthamiana* failed to detect MPK6 activation by EPF2 (ref. 17), probably due to a limitation of the heterologous co-expression system for capturing fast and transient response. We therefore tested MAPK activation *in vivo* using *Arabidopsis* seedlings. Application of mEPF2 peptide to *Arabidopsis* wild-type seedlings rapidly elicited phosphorylation of MPK3 and MPK6 in 10 min, a characteristic signature of MAPK activation, which declined after 2 h (Fig. 4a, b). Heat-induced denaturation of mEPF2 greatly diminished MAPK phosphorylation, correlating with its loss of bioactivity (Fig. 4b, c). By contrast, Stomagen peptide treatment failed to trigger MAPK phosphorylation (Fig. 4a). We conclude that EPF2 activates ER signalling, leading to subsequent MAPK activation to inhibit stomatal development, while Stomagen prevents the signal transduction.

Discussion

Our work elucidates the competitive binding of Stomagen and EPF2 to ER as a molecular mechanism optimizing stomatal patterning. Plant genomes possess large numbers of peptide gene families, the functions of which remain largely unknown[23]. The concept of fine-tuning signal transduction by related endogenous peptides that assume opposing functions may extend to other peptide families. EPF2 is expressed in a subset of protodermal cells, while Stomagen is secreted from an underlying internal tissue[4,5,13,14]. Thus, it seems plausible that a protodermal cell might respond to differences in intrinsic concentrations of EPF2 and Stomagen on each neighbouring side. It remains to be tested whether local concentrations of Stomagen in the apoplast reflect the IC_{50} values we have determined biochemically (Fig. 3e). The complex effects of *STOMAGEN* overexpression on a series of *er*-family mutants in the *tmm* background (Fig. 2) resemble that of *challah* (*chal*) higher-order mutants, which lack EPFL4 and EPFL6 peptides, another set of ER ligands promoting stem growth[24–26]. This raises the possibility that complex fine-tuning of multiple EPF-family peptides may occur at developmental contexts far beyond stomatal patterning. Quantitative visualization of each peptide *in vivo* during epidermal development, as well as precise documentation of the dose–response effects of simultaneous mixed peptide applications of wide concentration gradients, may reveal the signalling complexity at the level of ligand–receptor association. EPF2 and Stomagen bind to ER and TMM with a similar affinity (Fig. 3), suggesting the formation of co-receptor complexes, a hallmark of receptor activation and signal transduction in plant LRR-RKs in development and innate immunity response[27,28]. Future structural and cell biological studies may reveal the intricacy behind how a cell interprets conflicting signals to make decisions during developmental patterning.

Online Content Methods, along with any additional Extended Data display items and Source Data, are available in the online version of the paper; references unique to these sections appear only in the online paper.

Received 5 August 2014; accepted 14 May 2015.
Published online 17 June 2015.

1. Dorey, K. & Amaya, E. FGF signalling: diverse roles during early vertebrate embryogenesis. *Development* **137,** 3731–3742 (2010).
2. Fukuda, H. & Higashiyama, T. Diverse functions of plant peptides: entering a new phase. *Plant Cell Physiol.* **52,** 1–4 (2011).
3. Hara, K., Kajita, R., Torii, K. U., Bergmann, D. C. & Kakimoto, T. The secretory peptide gene EPF1 enforces the stomatal one-cell-spacing rule. *Genes Dev.* **21,** 1720–1725 (2007).
4. Hara, K. *et al.* Epidermal cell density is auto-regulated via a secretory peptide, EPIDERMAL PATTERNING FACTOR 2 in *Arabidopsis* leaves. *Plant Cell Physiol.* **50,** 1019–1031 (2009).
5. Hunt, L. & Gray, J. E. The signaling peptide EPF2 controls asymmetric cell divisions during stomatal development. *Curr. Biol.* **19,** 864–869 (2009).
6. Lee, J. S. *et al.* Direct interaction of ligand-receptor pairs specifying stomatal patterning. *Genes Dev.* **26,** 126–136 (2012).
7. Shpak, E. D., McAbee, J. M., Pillitteri, L. J. & Torii, K. U. Stomatal patterning and differentiation by synergistic interactions of receptor kinases. *Science* **309,** 290–293 (2005).
8. Nadeau, J. A. & Sack, F. D. Control of stomatal distribution on the *Arabidopsis* leaf surface. *Science* **296,** 1697–1700 (2002).
9. Wang, H., Ngwenyama, N., Liu, Y., Walker, J. & Zhang, S. Stomatal development and patterning are regulated by environmentally responsive mitogen-activated protein kinases in *Arabidopsis*. *Plant Cell* **19,** 63–73 (2007).
10. Lampard, G. R., Macalister, C. A. & Bergmann, D. C. *Arabidopsis* stomatal initiation is controlled by MAPK-mediated regulation of the bHLH SPEECHLESS. *Science* **322,** 1113–1116 (2008).

11. Bemis, S. M., Lee, J. S., Shpak, E. D. & Torii, K. U. Regulation of floral patterning and organ identity by *Arabidopsis* ERECTA-family receptor kinase genes. *J. Exp. Bot.* **64,** 5323–5333 (2013).
12. Bergmann, D. C., Lukowitz, W. & Somerville, C. R. Stomatal development and pattern controlled by a MAPKK kinase. *Science* **304,** 1494–1497 (2004).
13. Sugano, S. S. *et al.* Stomagen positively regulates stomatal density in *Arabidopsis*. *Nature* **463,** 241–244 (2010).
14. Kondo, T. *et al.* Stomatal density is controlled by a mesophyll-derived signaling molecule. *Plant Cell Physiol.* **51,** 1–8 (2010).
15. Hunt, L., Bailey, K. J. & Gray, J. E. The signalling peptide EPFL9 is a positive regulator of stomatal development. *New Phytol.* **186,** 609–614 (2010).
16. Ohki, S., Takeuchi, M. & Mori, M. The NMR structure of stomagen reveals the basis of stomatal density regulation by plant peptide hormones. *Nat. Commun.* **2,** 512 (2011).
17. Jewaria, P. K. *et al.* Differential effects of the peptides Stomagen, EPF1 and EPF2 on activation of MAP kinase MPK6 and the SPCH protein level. *Plant Cell Physiol.* **54,** 1253–1262 (2013).
18. Geisler, M., Yang, M. & Sack, F. D. Divergent regulation of stomatal initiation and patterning in organ and suborgan regions of the *Arabidopsis* mutants *too many mouths* and *four lips*. *Planta* **205,** 522–530 (1998).
19. Pillitteri, L. J., Bogenschutz, N. L. & Torii, K. U. The bHLH protein, MUTE, controls differentiation of stomata and the hydathode pore in *Arabidopsis*. *Plant Cell Physiol.* **49,** 934–943 (2008).
20. Okuda, S. *et al.* Defensin-like polypeptide LUREs are pollen tube attractants secreted from synergid cells. *Nature* **458,** 357–361 (2009).
21. Gómez-Gómez, L. & Boller, T. FLS2: An LRR receptor-like kinase involved in the perception of the bacterial elicitor flagellin in *Arabidopsis*. *Mol. Cell* **5,** 1003–1011 (2000).
22. Zipfel, C. *et al.* Bacterial disease resistance in *Arabidopsis* through flagellin perception. *Nature* **428,** 764–767 (2004).
23. Hanada, K. *et al.* Small open reading frames associated with morphogenesis are hidden in plant genomes. *Proc. Natl Acad. Sci. USA* **110,** 2395–2400 (2013).
24. Abrash, E. B. & Bergmann, D. C. Regional specification of stomatal production by the putative ligand CHALLAH. *Development* **137,** 447–455 (2010).
25. Abrash, E. B., Davies, K. A. & Bergmann, D. C. Generation of signaling specificity in *Arabidopsis* by spatially restricted buffering of ligand-receptor interactions. *Plant Cell* **23,** 2864–2879 (2011).
26. Uchida, N. *et al.* Regulation of inflorescence architecture by intertissue layer ligand-receptor communication between. *Proc. Natl Acad. Sci. USA* **109,** 6337–6342 (2012).
27. Santiago, J., Henzler, C. & Hothorn, M. Molecular mechanism for plant steroid receptor activation by somatic embryogenesis co-receptor kinases. *Science* **341,** 889–892 (2013).
28. Sun, Y. *et al.* Structural basis for flg22-induced activation of the *Arabidopsis* FLS2–BAK1 immune complex. *Science* **342,** 624–628 (2013).

Supplementary Information is available in the online version of the paper.

Acknowledgements We thank I. Hara-Nishimura for *STOMAGEN-ami* lines and anti-Stomagen antibody; K. Peterson for *iSTOMAGEN* construct and transgenic lines; M. Kanaoka and N. Kamiya for LURE2 peptides; D. Baulcombe for p19 plasmid; C. Tamerler and M. Sarikaya for use of the HPLC, QCM and MALDI-ToF equipment; A. Hofstetter for technical assistance; and J. McAbee, K. Peterson, T. Imaizumi, B. Wakimoto, S. Di Rubbo and R. Horst for comments. K.U.T. is an HHMI-GBMF Investigator and an Endowed Distinguished Professor of Biology; J.S.L. was an NSERC Postdoctoral Fellow. Y.-C.L.L. was a Mary Gates Undergraduate Research Fellow of the University of Washington.

Author Contributions J.S.L. and K.U.T. conceived the project. J.S.L., M.H., M.M., J.A. and Y.-C.L.L. purified peptides and performed ligand–receptor binding and bioassays. J.S.L and S.-K.H. performed RT–PCR. J.S.L. and A.P. performed MAPK assays. J.S.L. and Y.-C.L.L. performed quantitative analysis of stomatal phenotypes. K.U.T. constructed *STOMAGEN* cDNA plasmid. K.U.T., J.S.L., M.H., M.M., Y.-C.L.L., A.P. and S.-K.H. analysed the data. K.U.T. wrote the manuscript with inputs from all co-authors.

Author Information Reprints and permissions information is available at www.nature.com/reprints. The authors declare no competing financial interests. Readers are welcome to comment on the online version of the paper. Correspondence and requests for materials should be addressed to K.U.T. (ktorii@u.washingotn.edu).

METHODS

No statistical methods were used to predetermine sample size.

Plant materials and growth conditions. The *Arabidopsis* accession Columbia (Col) was used as wild type. All plants used in this study are in the Col background. The following mutants and transgenic plant lines were reported previously: *er-105*, *erl1-2*, *erl2-1* and their higher order mutants[7]; *tmm-1* (ref. 8); *epf1*, *epf2*, *epf1 epf2* and *tmm-KO* (refs 3, 4); *ER(ΔK)* in *er-105*, *ERL1(ΔK)* in *erl1-2* (ref. 6); and *STOMAGEN-ami* line (line 12; a gift from I. Hara-Nishimura)[13]. The *STOMAGEN-ami* lines were introduced into various mutant or transgenic backgrounds via genetic crosses. Plants were grown as described previously[29]. For phenotypic analysis, seedlings were grown on 0.5 Murashige and Skoog (MS) media containing 1× Gamborg Vitamin (Sigma), 0.75% Bacto Agar, and 1% w/v sucrose under continuous light condition at 50 μmol s^{-1} m^{-2} (light intensity measured by LI-250A; LI-COR).

Plasmid construction and transgenic plants generation. pKUT608 (pENTR-*STOMAGEN*) and pKMP127 (*Est::STOMAGEN*) were generated. See Extended Data Table 1 for plasmid and primer sequence information. Transgenic *Arabidopsis* plants were generated by the floral dip method[30]. Multiple transgenic lines per construct were subjected to phenotypic characterization and representative lines (three lines if lines were established, and 12–14 lines if T1 lines were used) were used for quantitative analyses. The *Est::STOMAGEN* lines were introduced into various mutants or transgenic backgrounds via genetic crosses.

Chemical induction of transgene. Transgenic *Arabidopsis* seedlings carrying *Est::STOMAGEN* was germinated on 0.5 MS medium supplemented with 10 μM oestradiol (Sigma). Induction of *STOMAGEN* gene expression (*iSTOMAGEN*) was confirmed by RT–PCR (see Extended Data Fig. 2). The induction was further confirmed by observing the epidermal phenotypes of cotyledons and hypocotyls using a confocal microscope.

RT–PCR analysis. RNA extraction, cDNA synthesis and RT–PCR were performed as previously described[31]. For a list of primers, see Extended Data Table 1.

Histology, microscopy and image analysis. Confocal microscopy images were taken using either Zeiss LSM700 operated by Zen2009 (Zeiss) described previously[6] or Leica SP5-WLL operated by LAS AF (Leica). Cell outlines were visualized with either propidium iodide (PI: Molecular Probes) or FM4-64 (Invitrogen) and observed using the HyD detector with excitation 515 nm, emission 623–642 nm. The images were false coloured using Photoshop CS6 (Adobe). Clearing of seedlings by chloral hydrate and observation using differential interference contrast (DIC) microscope was performed as described previously[32]. For histological analysis, seedlings were stained with toluidine blue-O (TBO: Sigma) as follows. Briefly, samples were placed in 9:1 v/v ethanol to acetic acid overnight, rehydrated through reduced ethanol series to deionized water, then stained with 0.5% TBO for 3 min. Seedlings were immediately rinsed with deionized water and subsequently mounted in 15% v/v glycerol. For bright-field and DIC microscopy, images were taken under Olympus BX51 equipped with DP73 digital camera operated by CellSens Standard software (Olympus).

Quantitative analysis of epidermis. Abaxial cotyledons from 10-day-old seedlings of respected genotypes were subjected to TBO staining or DIC microscopy. The central regions overlying the distal vascular loop were imaged and numbers of epidermal cells, stomata and their cluster size were quantified. For each genotype, sample size of 14–16 was used and over 1,000 epidermal cells were counted to provide statistical robustness. For cotyledons of *Est::STOMAGEN* lines, individual T1 seedlings were subjected to analysis. For hypocotyls, three representative T2 *Est::STOMAGEN* lines were analysed. For each seedling, a representative image was taken at the exact location to minimize the variance. Specific numbers of stomata are listed for each genotype in corresponding figure legends. Statistical analysis (Wilcoxon rank sum test) was performed using R version 3.0.3 for stomatal density, stomatal index and SLGC index. *P* values are indicated in each figure legend.

Transient protein expression in *Nicotiana benthamiana*. *Agrobacterium tumefaciens* strain GV3101 was transformed with expression clones and grown in yeast extract and beef medium supplemented with relevant antibiotics. Bacterial cultures were precipitated and resuspended in infiltration medium (10 mM $MgCl_2$, 10 mM MES (pH 5.6) and 150 μM acetosyringone). Culture densities were adjusted to an OD_{600} of 1.0, and the cells were incubated at room temperature for 4 h before infiltration. Equal volumes of cultures carrying different constructs were mixed. To enhance transient expression in tobacco, the silencing suppressor p19 (a gift from D. Baulcombe) was co-infiltrated[33]. The bacterial suspensions were infiltrated into young but fully expanded leaves of *N. benthamiana* plants. After infiltration, plants were cultivated at 25 °C and collected for further biochemical assays after 48–72 h.

Peptide expression, purification and refolding. Recombinant mEPF2 peptide was prepared as reported previously[6] and the mature Stomagen peptide, either wild-type or non-refolding mutant version in which all six cysteines were substituted by serines, were chemically synthesized (Invitrogen and BioSynthesis). The Stomagen peptide was dissolved in 20 mM Tris-HCl, pH 8.8, and 50 mM NaCl and refolded (Mini dialysis kit, MWCO:1,000, GE Healthcare) for 3 d at 4 °C using glutathione (reduced and oxidized forms; Wako) and L-arginine ethyl ester dihydrochloride (Sigma). The peptides were further dialysed three times against 50 mM Tris-HCl, pH 8.0 for 1.5 d to remove glutathione. For non-folding mutant Stomagen, chemically synthesized peptides were dissolved in 50 mM Tris-HCl, pH 8.0. The resulting mEPF2, Stomagen and mutant Stomagen peptides were fractionated using C18 column (Gemini) by HPLC (Waters Delta Prep 3000 HPLC) as previously described to determine the purity of each peptide[6]. The separated peaks were collected, and each peak was identified by MALDI-TOF mass spectrometry on an Autoflex II mass spectrometer in positive ion mode (Bruker Daltonics) using 2:1 a-cyano-4-hydroxycinnamic acid and 2,5-dihydroxy-benzoic acid matrix. The collected HPLC-purified mEPF2 and Stomagen peptide peaks were freeze-dried, then re-dissolved to appropriate concentration. Quantification of the active populations of peptides was determined using NanoDrop8000 (Thermo Scientific) using the following molar extinction coefficients: Stomagen, 5,960; EPF2, 6,460; LURE2, 23,950 mol^{-1} cm^{-1}. For bioassays, freeze-dried peptides were re-dissolved to appropriate concentration in MS medium. For subsequent biochemical assays, the amounts of bioactive peptides were calculated from this quantification.

Peptide bioassays. Refolded recombinant mEPF2 and Stomagen peptides in buffer were applied to 1-day-old *Arabidopsis* plants that had germinated on 0.5 MS medium. After 5 d of further incubation in 0.5 MS liquid medium containing each peptide (2.5–5 μM concentration), stomatal phenotypes of abaxial cotyledon epidermis were determined by inspection with a confocal microscope as described previously[6].

Immunoprecipitation, protein gel electrophoresis and immunoblots. For immunoprecipitation and co-immunoprecipitation assays, *N. benthamiana* leaves expressing CaMV35S::ERΔK–GFP, CaMV35S::FLS2(ΔK)–GFP, CaMV35S::TMM–GFP, CaMV35S::GFP, or empty vector were subjected to protein preparation (microsomal fraction enrichment for all except soluble GFP). Co-incubation with Stomagen (1 μM) or LURE2 peptides (1 μM) and immunoprecipitation procedure are described in the Ligand Competition Assays section below. Immunoprecipitation using either anti-GFP (Abcam ab290) antibodies and protein gel immunoblot (western blot) analysis using anti-GFP (Invitrogen C163), anti-Flag (Sigma-Aldrich M2), anti-His (Qiagen anti-His5 34660), and anti-Stomagen (a gift from I. Hara-Nishimura)[13] antibodies were performed as described previously[6]. As secondary antibodies, either goat anti-mouse (GE Healthcare NA931) or anti-rabbit IgG horseradish peroxidase-linked antibodies (Sigma A6154) were used at a dilution of 1:50,000. The protein blots were visualized using SuperSignal West Femto Maximum Sensitivity Substrate (Thermo Scientific).

Quartz crystal microbalance. QCM measurements were performed using QCM-Z500 (KSV Instruments) and commercially available AT-cut polished QCM crystals with a fundamental resonant frequency of 4.95 MHz (International Crystal Manufacturing Co.) as reported previously[6]. The QCM crystal chips were pre-treated with anti-GFP antibody (Abcam ab290) to functionalize the chip surface. Subsequently, GFP-tagged receptors or GFP expressed in *N. benthamiana* and extracted as a microsomal fraction (for ER(ΔK)–GFP and TMM–GFP) or a total fraction (GFP) were immobilized onto a QCM sensor chip via anti-GFP antibody linkage. The chips were washed with a phosphate buffer extensively. After establishing a stable baseline using phosphate buffer solution, purified bioactive mEPF2 or Stomagen peptides in the phosphate buffer was added stepwise to the QCM chamber. The frequency change for QCM was monitored until no further change was observed, indicating equilibrium. All experiments were performed at 4 °C in stop-flow mode. The peptide–receptor binding was quantified via QCM by measuring the frequency shifts, ΔF, at several peptide concentrations. To determine the dissociation constant (K_d) of each peptide–receptor pair, the experimental frequency shift values were fitted to the Langmuir adsorption model: $-\Delta F = \Delta F_{max} C/(C + K_d)$, where ΔF_{max} is the frequency shift when the binding is saturated and C is the concentration of the bulk solution, using a least squares regression.

Ligand competition assays. *N. benthamiana* leaves expressing *CaMV35S::ER(ΔK)–GFP* were ground in liquid nitrogen and homogenized in extraction buffer (100 mM Tris-HCl pH 8.8, 150 mM NaCl, 1 mM EDTA, 20% glycerol, 20 mM NaF, 1 mM PMSF, 1:1,000 Complete protease inhibitor cocktail (Roche Applied Science)). The slurry was centrifuged at 10,000*g* for 15 min at 4 °C. The supernatant was sonicated on ice and then centrifuged at 100,000*g* for 30 min at 4 °C to give a pellet of the microsomal fractions. The pellet was resuspended in membrane solubilization buffer (100 mM Tris-HCl at pH 7.3, 150 mM NaCl, 1 mM EDTA, 10% glycerol, 1% Triton X-100, 20 mM NaF, 1 mM

PMSF, 1:1,000 Complete protease inhibitor cocktail) to release membrane proteins. The solution was sonicated on ice and centrifuged again at 100,000*g* for 30 min at 4 °C. The supernatant was incubated with Protein-G-coupled magnetic beads (Dynabeads Protein G, Invitrogen) that captured anti-GFP (ab290; Abcam) antibody at 4 °C for 2 h with gentle agitation. Then, the beads were washed four times with 500 µl of phosphate buffer (pH 7.4). The immunoprecipitates were suspended in 500 µl of binding buffer (50 mM MES-KOH, pH 5.5 with 100 mM sucrose) containing 1 µM mEPF2–MYC–HIS peptide in the absence or presence of different concentration of unlabelled bioactive Stomagen peptide and then incubated at 4 °C for 1 h with gentle agitation. The reaction mixture was washed four times with 500 µl of phosphate buffer (pH 7.4) to separate bound and free mEPF2–MYC–His peptide, and precipitated proteins were eluted with 2× SDS sample buffer at 80 °C for 5 min. Either total membrane or immunoprecipitated proteins were separated on a SDS–PAGE gel and transferred to PDVF membrane (Millipore) for immunoblot analysis using monoclonal anti-GFP (C163, 1:1,000, Invitrogen), anti-MYC (ab32, 1:1,000, abcam) or anti-Stomagen antibodies (1:5,000, a gift from I. Hara-Nishimura)[13] as primary antibodies. As secondary antibodies, either goat anti-mouse or rabbit IgG horseradish peroxidase-linked antibodies (GE Healthcare NA931; Sigma A6154) were used at a dilution of 1:50,000. Co-immunoprecipitated mEPF2 was detected first. Then, the same blot was re-probed with anti-Stomagen antibody to detect Stomagen.

Four biological replicates were performed and subjected to quantification of the IC_{50} values as the following. Band intensities on western blots were quantified using IMAGEJ (http://rsb.info.nih.gov/ij/index.html). Pixel values were measured on equal-sized areas and normalized against the bands detecting same immunoprecipitates by monoclonal anti-GFP antibody. The intensity values shown in the paper are the ratios relative to the references, and values were analysed by nonlinear regression analysis using OriginLab version 6 (OriginLab) to calculate the IC_{50} value.

MAPK phosphorylation assays. 12-day-old *Arabidopsis* seedlings were grown for 5 days on 0.5 MS media plates and then transferred to 0.5 MS liquid media in a 12-well cluster plate (Falcon 3047). Seedlings were treated with buffer only, mEPF2 (2.5 µM), or with Stomagen (5 µM) at room temperature before being pooled for harvest. For heat denaturation of mEPF2, the peptide solution was treated at 95 °C for 2 h before MAPK phosphorylation assays and bioassays. Plant materials were ground in liquid nitrogen, and then extracted with buffer (100 mM HEPES, pH 7.5, 5 mM EDTA, 5 mM EGTA, 2 mM DTT, 10 mM Na_3VO_4, 10 mM NaF, 50 mM β-glycerolphosphate, 1 mM PMSF, 1 tablet per 50 ml extraction buffer of proteinase inhibitor mixture, 10% glycerol, 7.5% (w/v) PVPP). After centrifugation at 13,000 r.p.m. for 30 min, the protein concentration was determined using a Bradford assay (Bio-Rad). Immunoblot analysis was performed using anti-phospho-ERK (1:2,000, Cell Signaling) antibody as primary antibody, and peroxidase-conjugated goat anti-rabbit IgG (1:15,000, Sigma) as secondary antibody.

29. Shpak, E. D., Lakeman, M. B. & Torii, K. U. Dominant-negative receptor uncovers redundancy in the *Arabidopsis* ERECTA leucin-rich repeat receptor-like kinase signaling pathway that regulates organ shape. *Plant Cell* **15,** 1095–1110 (2003).
30. Clough, S. J. & Bent, A. F. Floral dip: a simplified method for *Agrobacterium*-mediated transformation of *Arabidopsis thaliana*. *Plant J.* **16,** 735–743 (1998).
31. Pillitteri, L. J., Peterson, K. M., Horst, R. J. & Torii, K. U. Molecular profiling of stomatal meristemoids reveals new component of asymmetric cell division and commonalities among stem cell populations in *Arabidopsis*. *Plant Cell* **23,** 3260–3275 (2011).
32. Pillitteri, L. J., Sloan, D. B., Bogenschutz, N. L. & Torii, K. U. Termination of asymmetric cell division and differentiation of stomata. *Nature* **445,** 501–505 (2007).
33. Voinnet, O., Rivas, S., Mestre, P. & Baulcombe, D. An enhanced transient expression system in plants based on suppression of gene silencing by the p19 protein of tomato bushy stunt virus. *Plant J.* **33,** 949–956 (2003).

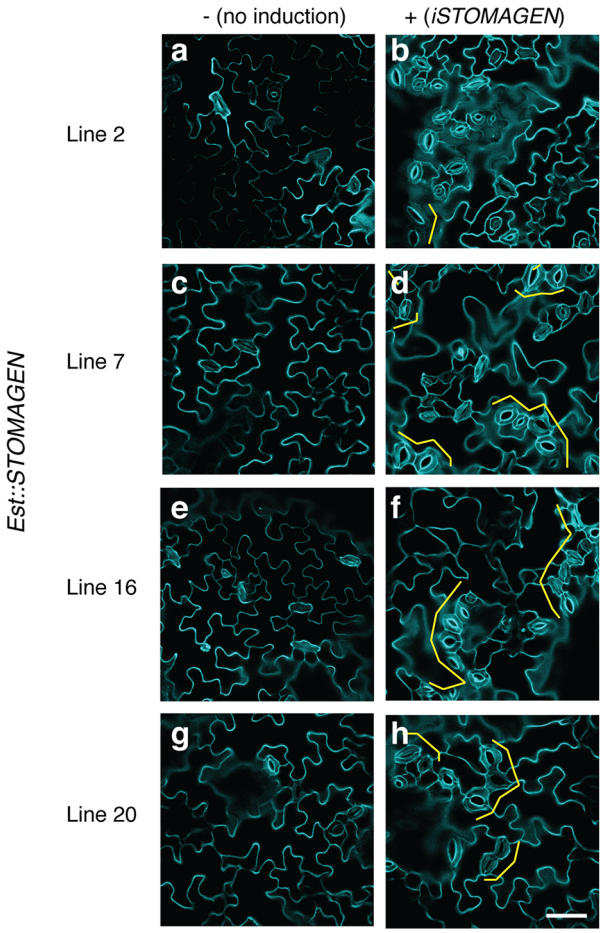

Extended Data Figure 1 | Stomatal clustering phenotype of induced *STOMAGEN* overexpression in multiple independent transgenic lines. Shown are confocal microscopy images of abaxial cotyledon epidermis from 10-day-old light-grown seedlings of four independent transgenic lines carrying an oestradiol-inducible *STOMAGEN* overexpression construct (*iSTOMAGEN*). Left panels, no induction (control); right panels, oestradiol induction; each row shows representative images from individual lines. Yellow brackets indicate stomatal clusters. Images are taken under the same magnification. Scale bar, 40 μm. $n = 3$ for each panel.

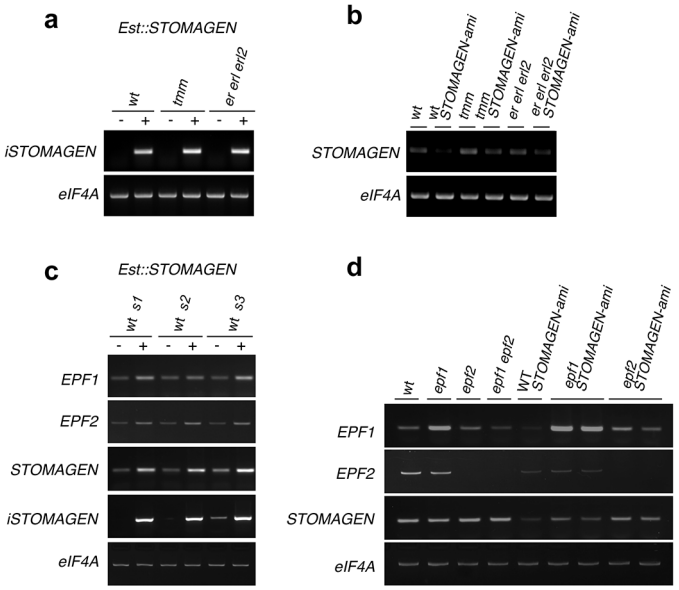

Extended Data Figure 2 | RT–PCR analysis of *STOMAGEN* transcripts in transgenic lines used in this study. **a**, Expression of oestradiol-inducible *STOMAGEN* transgene (*iSTOMAGEN*) in transgenic lines expressing oestradiol-inducible *STOMAGEN* overexpression (*Est::STOMAGEN*) lines from wild-type (wt), *tmm* and *er erl1 erl2* triple mutant background with or without oestradiol induction. **b**, Expression of the endogenous *STOMAGEN* transcripts in each genotype carrying *STOMAGEN-ami* construct. *tmm* or *er erl1 erl2* mutation does not seem to affect *STOMAGEN* transcript levels. **c**, Expression of *EPF1*, *EPF2*, total *STOMAGEN* and *STOMAGEN* transgene (*iSTOMAGEN*) transcripts in transgenic *Est::STOMAGEN* lines (in two different T1 populations (s1 and s2) and a representative T3 line (s3)) with or without oestradiol induction. *STOMAGEN* overexpression by oestradiol causes modest increase in *EPF1* and *EPF2* transcripts, which accords with increased stomatal differentiation by *iSTOMAGEN*. **d**, *EPF1*, *EPF2* and *STOMAGEN* transcript accumulation in wild-type (wt) and single- and higher-order loss-of-function mutants of *epf1*, *epf2* and *stomagen* (*STOMAGEN-ami*). For *epf1 STOMAGEN-ami* and *epf2 STOMAGEN-ami* lines, two different F_3 populations derived from the same genetic crosses were used to test the reproducibility. *STOMAGEN* expression is not influenced by *epf1* and *epf2* mutations, consistent with the proto-mesophyll expression of *STOMAGEN*. However, EPF2 expression is reduced by *STOMAGEN-ami*, consistent with reduced stomatal cell lineages by *STOMAGEN* co-suppression. As reported, *epf1* has a T-DNA insertion within the 5′ UTR[3], which results in accumulation of aberrant transcripts. For all experiments, *elF4A* was used as a control. For primer sequences see Extended Data Table 1.

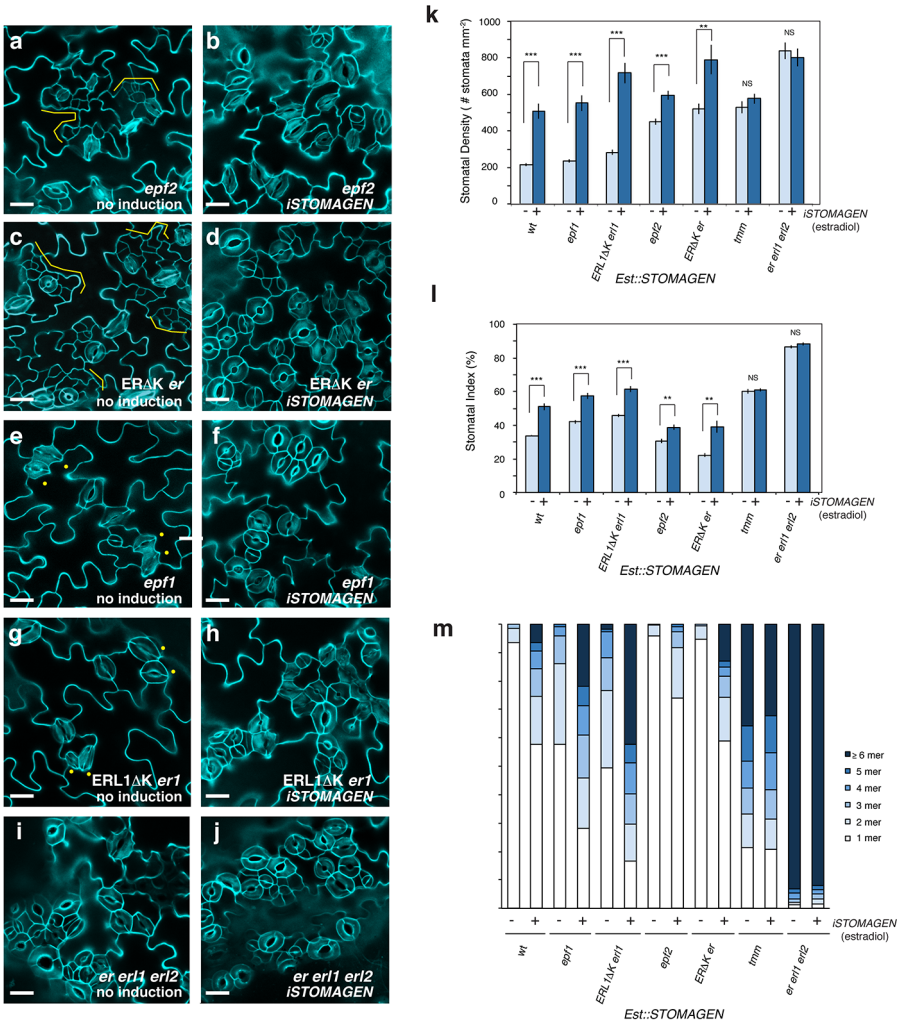

Extended Data Figure 3 | *STOMAGEN* overexpression promotes stomatal differentiation in genetic backgrounds missing/blocking EPF2–ER and EPF1–ERL1 signalling components. **a**–**j**, Representative confocal images of cotyledon abaxial epidermis from 10-day-old light-grown transgenic seedlings of the following genotypes, each carrying *Est::STOMAGEN* construct: *epf2* (**a**, **b**); dominant-negative ER (ER(ΔK)) in *er* (**c**, **d**); *epf1* (**e**, **f**); dominant-negative ERL1 (ERL1(ΔK)) in *erl1* (**g**, **h**); *er erl1 erl2* (**i**, **j**). For each genotype, a control uninduced phenotype (**a**, **c**, **e**, **g**, **i**) and induced *STOMAGEN* overexpression (*iSTOMAGEN*) (**b**, **d**, **f**, **h**, **j**) are shown. Blocking ER or lacking EPF2 produces small stomatal-lineage cells due to excessive entry divisions (**a, c**; yellow brackets). *iSTOMAGEN* confers stomatal clusters and small stomatal-lineage cells are no longer present (**b** and **d**). Blocking ERL1 or lacking EPF1 causes a stomatal pairing due to a violation of one-cell-spacing rule (**e**, **g**; dots). *iSTOMAGEN* enhances stomatal cluster phenotype in these genotypes (**f**, **h**). *iSTOMAGEN* does not enhance stomatal clustering defects in *er erl1 erl2* (**i**, **j**). Images were taken under the same magnification. Scale bars, 30 μm. $n = 29$ (**a**); $n = 24$ (**b**); $n = 16$ (**c**); $n = 17$ (**d**); $n = 22$ (**e**); $n = 23$ (**f**); $n = 17$ (**g**); $n = 20$ (**h**); $n = 24$ (**i**); $n = 24$ (**j**). **k**–**m**, Stomatal density (number of stomata per mm^2) (**k**); stomatal index (% of number of stomata per stomata + non-stomatal epidermal cells) (**l**); and stomatal cluster distribution (in %) (**m**) from 10-day-old abaxial cotyledons of transgenic lines of each genotype carrying *Est::STOMAGEN* construct. −, no induction; +, induced by 10 μM oestradiol. Stomagen overexpression significantly increases stomatal density in all genotypes except for *er erl1 erl2* and *tmm*. Error bars indicate s.e.m. $***P < 0.001$; $**P < 0.01$; NS, not significant; Welch 2-sample *t*-test. Number of seedlings subjected to analysis, $n = 14$–16. Total numbers of stomata counted: wt, no induction 1,277, induction 2,639; *epf1*, no induction 1,390, induction 3,485; *ERL1(ΔK) erl1*, no induction 1,573, induction 3,991; *epf2*, no induction 2,502, induction 3,317; *ER(ΔK) er*, no induction 2,899, induction 4,397; *tmm*, no induction 2,948, induction 3,212; *er erl1 erl2*, no induction 4,454, induction 4,464. All genotypes carry *Est::STOMAGEN*. wt, no induction $n = 16$, induction $n = 14$; *epf1*, no induction $n = 16$, induction $n = 17$; *ERL1(ΔK) erl1*, no induction $n = 15$, induction $n = 15$; *epf2*, no induction $n = 15$, induction $n = 15$; *ER(ΔK) er*, no induction $n = 15$, induction $n = 15$; *tmm*, no induction $n = 15$, induction $n = 15$; *er erl1 erl2*, no induction $n = 15$, induction $n = 15$.

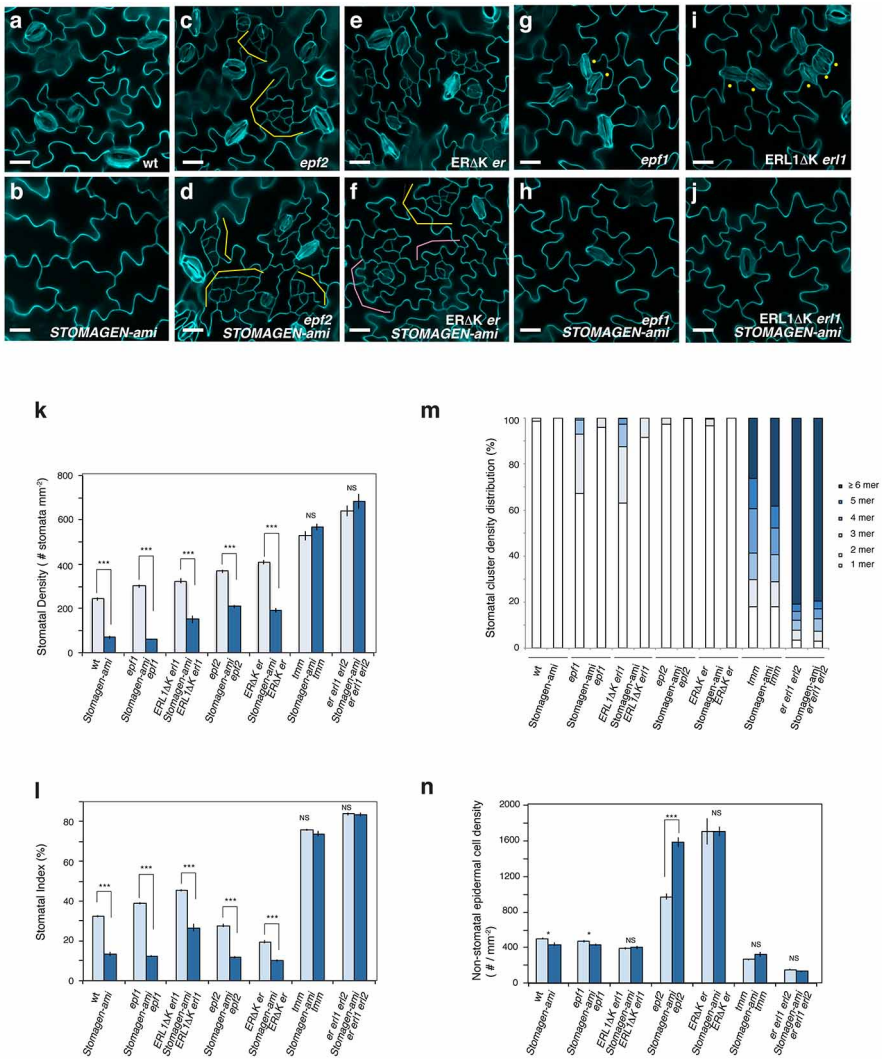

Extended Data Figure 4 | *STOMAGEN* co-suppression results in reduced stomatal development in genetic backgrounds missing or blocked in EPF2–ER and EPF1–ERL1 signalling pathways. **a**–**j**, Representative confocal images of cotyledon abaxial epidermis from 10-day-old light-grown transgenic seedlings of the following genotypes: wild type (**a**); *STOMAGEN-ami* (**b**); *epf2* (**c**); *epf2 STOMAGEN-ami* (**d**); dominant-negative ER (*ER(ΔK)*) in *er* (**e**); *ER(ΔK) er STOMAGEN-ami* (**f**); *epf1* (**g**); *epf1 STOMAGEN-ami* (**h**); dominant-negative ERL1 (*ERL1(ΔK)*) in *erl1* (**i**); *ERL1(ΔK) erl1 STOMAGEN-ami* (**j**). *STOMAGEN-ami* markedly reduces stomatal differentiation in wild type (**a**, **b**). Blocking ER or lacking EPF2 produces small stomatal-lineage cells due to excessive entry divisions (**c**, **e**; yellow brackets). *STOMAGEN-ami* exaggerates the small stomatal-lineage cells of *epf2* (**d**; yellow brackets). *STOMAGEN-ami* ER(ΔK) *er* shows excessive asymmetric entry as well as amplifying divisions (**f**; yellow and pink brackets, respectively). Blocking ERL1 or lacking EPF1 causes a stomatal pairing due to a violation of one-cell-spacing rule (**g**, **i**; dots). *STOMAGEN-ami* suppresses these mild stomatal pairing phenotypes and reduces stomatal differentiation (**h**, **j**). Images were taken under the same magnification. Scale bars, 30 μm. $n = 13$ (**a**); $n = 26$ (**b**); $n = 15$ (**c**); $n = 23$ (**d**); $n = 11$ (**e**); $n = 17$ (**f**); $n = 12$ (**g**); $n = 22$ (**h**); $n = 18$ (**i**); $n = 13$ (**j**). **k**–**n**, Stomatal density (**k**), stomatal index (**l**), stomatal cluster distribution (in %; **m**), and non-stomatal epidermal cell density (**n**) from 10-day-old abaxial cotyledons of each genotype with or without carrying *STOMAGEN-ami* construct. Error bars, s.e.m. $***P < 0.001$; $*P \leq 0.05$; NS, not significant; Welch 2-sample *t*-test. $n = 9$–16. Total numbers of stomata counted: wt, 719; *STOMAGEN-ami*, 204; *epf1*, 1,004; *epf1 STOMAGEN-ami*, 383; *ERL1(ΔK) erl1*, 1,558; *ERL1(ΔK) erl1 STOMAGEN-ami*, 504; *epf2*, 1,505; *epf2 STOMAGEN-ami*, 1,165; *ER(ΔK) er*, 1,361; *ER(ΔK) er STOMAGEN-ami*, 782; *tmm*, 2,495; *tmm STOMAGEN-ami*, 2,688; *er erl1 erl2*, 1,853; *er erl1 erl2 STOMAGEN-ami*, 2,028. Total numbers of non-stomatal epidermal cells counted: wt, 1,494; *STOMAGEN-ami*, 1,299; *epf1*, 1,584, *epf1 STOMAGEN-ami*, 2,711; *ERL1(ΔK) erl1*, 871; *ERL1(ΔK) erl1 STOMAGEN-ami*, 1,348; *epf2*, 3,980; *epf2 STOMAGEN-ami*, 8,808; *ER(ΔK) er*, 5,739; *ER(ΔK) er STOMAGEN-ami*, 6,939; *tmm*, 790; *tmm STOMAGEN-ami*, 962; *er erl1 erl2*, 479; *er erl1 erl2 STOMAGEN-ami*, 391. wt, $n = 8$; *STOMAGEN-ami*, $n = 8$; *epf1*, $n = 9$, *epf1 STOMAGEN-ami*, $n = 17$; *ERL1(ΔK) erl1*, $n = 13$; *ERL1(ΔK) erl1 STOMAGEN-ami*, $n = 9$; *epf2*, $n = 11$; *epf2 STOMAGEN-ami*, $n = 15$; *ER(ΔK) er*, $n = 9$; *ER(ΔK) er STOMAGEN-ami*, $n = 11$; *tmm*, $n = 8$; *tmm STOMAGEN-ami*, $n = 8$; *er erl1 erl2*, $n = 8$; *er erl1 erl2 STOMAGEN-ami*, $n = 8$.

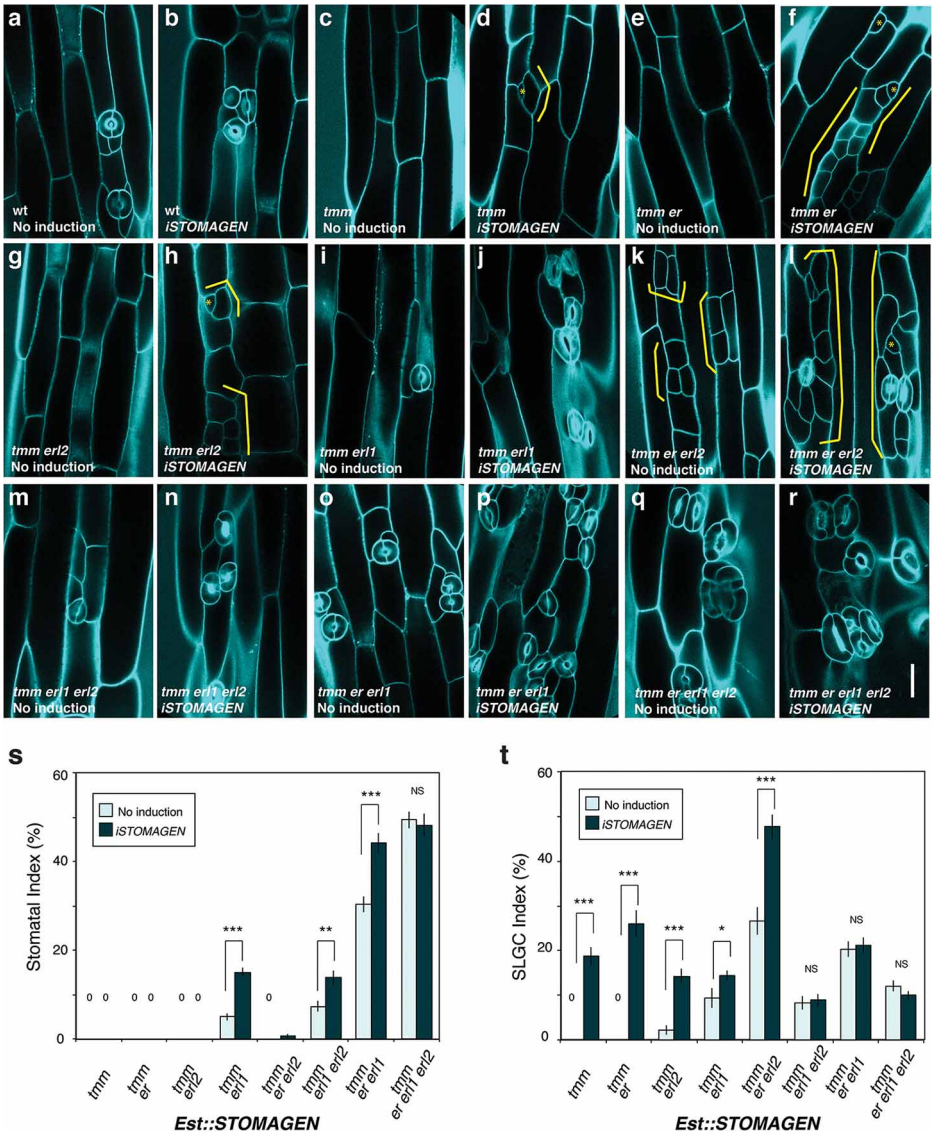

Extended Data Figure 5 | *STOMAGEN* overexpression on stomatal development in *tmm* hypocotyl epidermis with combinatorial loss-of-function in *ER*-family genes: a complete set. **a**–**r**, Representative confocal microscopy images of hypocotyl epidermis from 10-day-old light-grown transgenic seedlings of the following genotypes, each carrying *Est::STOMAGEN*: wild-type (wt) (**a**, **b**); *tmm* (**c**, **d**); *tmm er* (**e**, **f**); *tmm erl2* (**g**, **h**); *tmm erl1* (**i**, **j**); *tmm er erl2* (**k**, **l**); *tmm erl1 erl2* (**m**, **n**); *tmm er erl1* (**o**, **p**); and *tmm er erl1 erl2* (**q**, **r**). A control, uninduced phenotype (**a**, **c**, **e**, **g**, **i**, **k**, **m**, **o**, **q**); *iSTOMAGEN* (**b**, **d**, **f**, **h**, **j**, **l**, **n**, **p**, **r**). *iSTOMAGEN* results in arrested stomatal precursor cells (asterisks) and stomatal-lineage ground cells (SLGCs; brackets) in *tmm* hypocotyls (**d**). *iSTOMAGEN* triggers entry divisions in *tmm er* and *tmm erl2* (**f**, **h**; brackets), and exaggerate the SLGC clusters in *tmm er erl2* (**k**, **l**; brackets). Images were taken under the same magnification. Scale bar, 30 μm. $n = 19$ (**a**); $n = 19$ (**b**); $n = 20$ (**c**); $n = 20$ (**d**); $n = 19$ (**e**); $n = 22$ (**f**); $n = 20$ (**g**); $n = 17$ (**h**); $n = 18$ (**i**); $n = 19$ (**j**); $n = 19$ (**k**), $n = 21$ (**l**); $n = 17$ (**m**); $n = 20$ (**n**); $n = 19$ (**o**); $n = 21$ (**p**); $n = 20$ (**q**); $n = 20$ (**r**). **s**, **t**, Stomatal index and SLGC index. **s**, $***P < 0.0001$; $**P < 0.01$; $*P < 0.5$ (Wilcoxon rank sum test). NS, not significant. 0, no stomata or SLGC observed; $n = 15$. Total number of stomata and SLGCs counted; *tmm* non-induced, 0 and 0; induced, 0 and 211; *tmm er* non-induced, 0 and 0; induced, 0 and 308; *tmm erl2* non-induced, 0 and 32; induced, 0 and 171; *tmm erl1* non-induced, 58 and 116; induced, 142 and 138; *tmm er erl2* non-induced, 0 and 270; induced, 10 and 676; *tmm er erl1* non-induced, 422 and 283; induced, 817 and 422; *tmm erl1 erl2* non-induced, 72 and 83; induced, 163 and 97; *tmm er erl1 erl2* non-induced, 1,229 and 295; induced, 1,068 and 222. $n = 15$ for all genotypes (**s**, **t**).

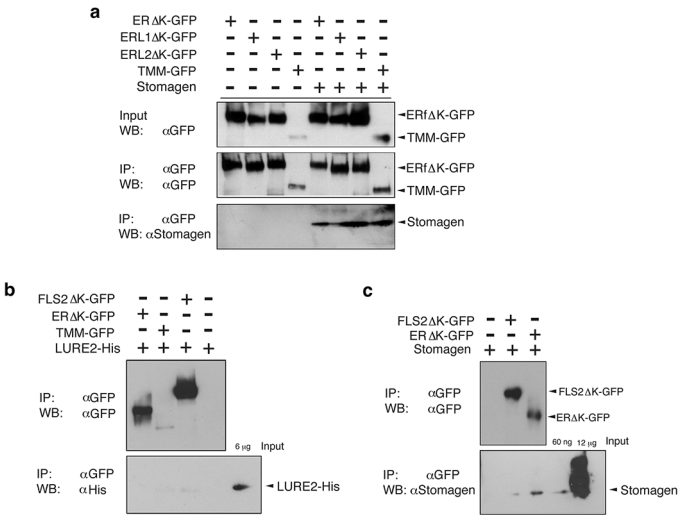

Extended Data Figure 6 | Association of Stomagen with ER-family receptors and TMM. a, Shown are co-immunoprecipitation assays of ligand–receptor pairs expressed in *N. benthamiana* leaves. The ectodomains and membrane-spanning domains of ER, ERL1 and ERL2 fused with GFP were separately expressed in *N. benthamiana*, and microsomal fractions were incubated with 1 μM Stomagen peptides followed by immunoprecipitation using anti-GFP (anti-GFP) antibody. Inputs and immunoprecipitates were immunoblotted using anti-GFP (anti-GFP) or anti-Stomagen (anti-Stomagen) antibodies. Experiments were repeated three times (three biological replicates). **b**, Co-immunoprecipitation of LURE2 peptide fused with hexa-histidine tag (LURE2–His) with *N. benthamiana* microsomal fractions expressing the ectodomains and membrane-spanning domains of ER and FLS2 fused with GFP, a full-length TMM fused with GFP, or a control, uninoculated leaf sample. Immunoprecipitation was performed using anti-GFP and immunoblotted using anti-GFP (for detection of receptors) or anti-His (for detection of LURE2–His) antibodies. Experiments were repeated twice (two biological replicates). **c**, Co-immunoprecipitation of Stomagen peptide with *N. benthamiana* microsomal fractions expressing the ectodomains and membrane-spanning domains of ER and FLS2 fused with GFP or a control, uninoculated leaf sample. Immunoprecipitation was performed using anti-GFP and immunoblotted using anti-GFP (for detection of receptors) or anti-Stomagen antibodies. Experiments were repeated four times (four biological replicates).

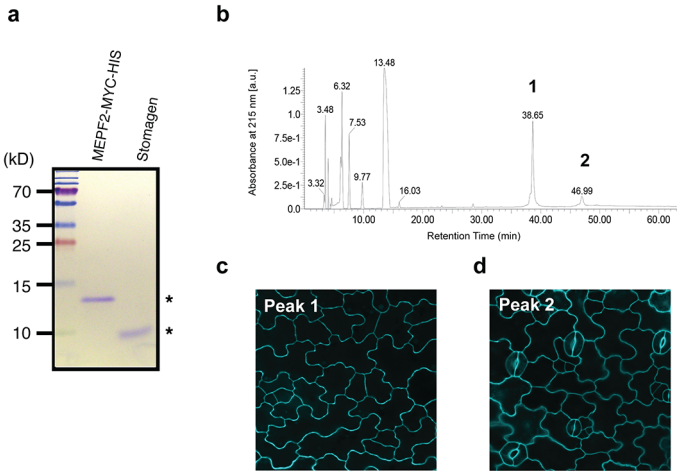

Extended Data Figure 7 | Purified mEPF2 and Stomagen recombinant peptides and separation of bioactive mEPF2 by reverse-phase chromatography. **a**, SDS–PAGE gel of purified and refolded mEPF2–MYC–HIS and Stomagen recombinant peptides (asterisks). Left: molecular mass markers. **b**, HPLC chromatogram of purified, refolded mEPF2. Peaks 1 and 2 in UV chromatogram were collected and subjected to bioassays. **c**, Confocal image of cotyledon epidermis from wild-type seedling grown a solution with peak 1 for 5 days. No stoma is visible, indicating that peak 1 contains bioactive mEPF2. Scale bar, 20 μm. $n = 19$. **d**, Confocal image of cotyledon epidermis from wild-type seedling grown in a solution with peak 2 for 5 days, with normal stomatal differentiation, indicating that the peptide is not bioactive. Scale bar, 20 μm. $n = 9$.

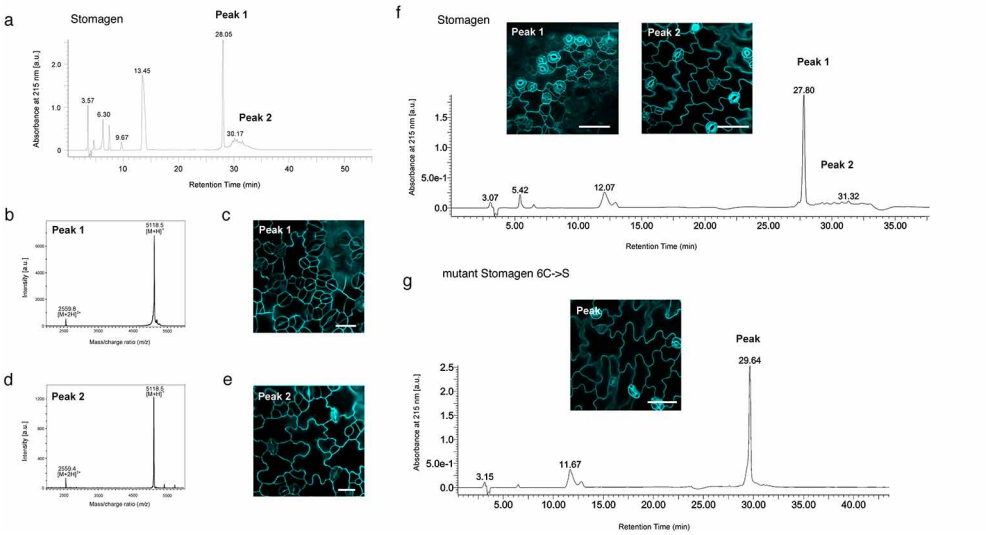

Extended Data Figure 8 | Separation of properly folded, bioactive Stomagen and mutant Stomagen peptides by reverse-phase chromatography followed by mass spectrometry and bioassays. **a**, HPLC chromatogram of purified, refolded Stomagen. Peaks 1 and 2 in UV chromatogram were collected and subjected to MALDI-TOF mass spectrometry (**b**, **d**) as well as for bioassays (**c**, **e**). **b**, MALDI-TOF spectrum of peak 1 from **a**. A single-charged peptide corresponding to synthetic Stomagen peptide was observed at $m/z = 5{,}118.5$ ($[M+H]^{+}$) and a double charged peptide at $m/z = 2{,}559.8$ ($[M+2H]^{2+}$). **c**, Confocal image of cotyledon epidermis from wild-type seedling grown a solution with peak 1. Severe stomatal clustering and overproduction of stomata are observed. Scale bar, 20 µm. $n = 8$. **d**, MALDI-TOF spectrum of peak 2 from **a**. **e**, Confocal image of cotyledon epidermis from wild-type seedling grown in a solution with peak 2 from **a**, with no stomatal clustering, indicating that the fraction is not bioactive. Scale bar, 20 µm. $n = 6$. **f**, HPLC chromatogram and bioassays of an independent batch of Stomagen peptides used for QCM analysis in direct comparison with non-folding mutant Stomagen peptides in Fig. 3c. Peaks 1 and 2 in UV chromatogram were collected and subjected for bioassays. Insets: confocal microscopy images of cotyledon epidermis from wild-type seedling grown a solution with peak 1 (bioactive) and peak 2 (non-active) for 5 days. Scale bars, 50 µm. $n = 8$ (peak 1); $n = 6$ (peak 2). **g**, HPLC chromatogram of purified, mutant Stomagen peptide in which all cysteine residues were substituted to serine residues (Stomagen_6C→S). The mutant Stomagen peptide yielded a single peak, which was subjected for bioassays followed by confocal microscopy (inset). No stomatal clustering was observed, indicating that non-folding Stomagen peptide is not bioactive, confirming the previous results[18]. Scale bar, 50 µm. $n = 8$ for each peptide treatment.

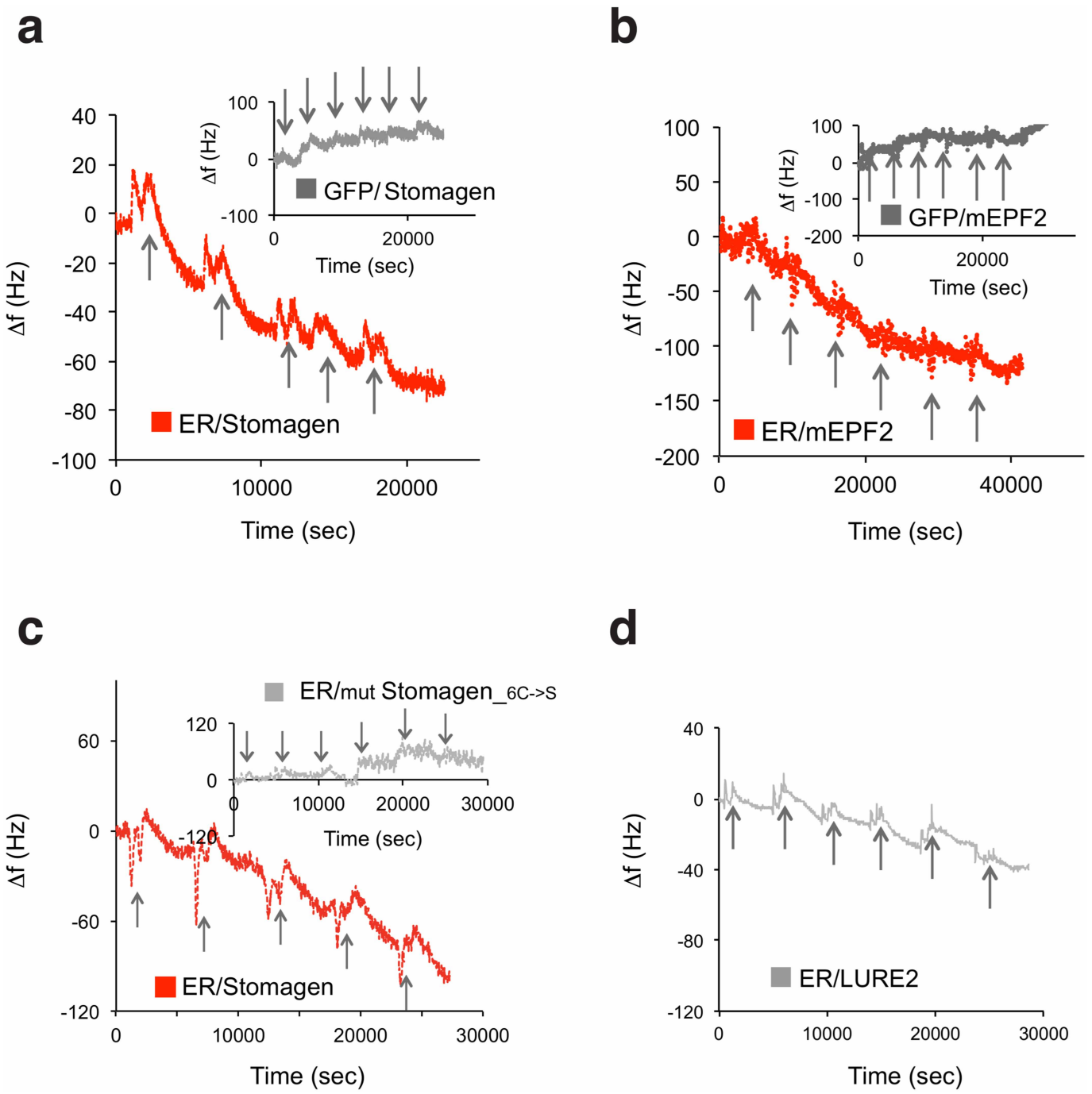

Extended Data Figure 9 | Raw QCM recording data. Shown are raw recording data of frequency shifts for representative QCM analysis using biosensor chips immobilized with ER(ΔK)–GFP and GFP (**a**, **b**, inset) after sequential injection of active Stomagen (**a**, **c**), mEPF2 (**b**), non-folding, inactive mutant Stomagen (**c**, inset), or LURE2 (**d**) in increasing concentrations. Bioactive Stomagen and inactive Stomagen experiments in **c** were performed side by side. Arrows indicate time of additional peptide application. Numbers of experiments performed for each analysis: Stomagen–ER, $n = 3$; Stomagen–TMM, $n = 2$; Stomagen–GFP, $n = 3$; mEPF2–ER, $n = 2$; mEPF2–TMM, $n = 3$; mEPF2–GFP, $n = 2$; inactive Stomagen_C6→S–ER, $n = 3$; and LURE2–ER, $n = 2$.

Extended Data Table 1 | List of plasmids and primers used in this study

Plasmid ID	Description	Insert	Vector	Bac R	Plant R
pKUT608	STOMAGEN in pENTR	STOMAGEN cDNA	pENTR	KAN	NA
pKMP127	proEst::STOMAGEN in pER8	STOMAGEN cDNA	pER8	SPEC/STREP	HYG
pJSL92	ERL2 genomic ΔKinase in pENTR	ERL2 genomic ΔKinase	pENTR	KAN	NA
pJSL93	35S::gERL2-ΔKinase-GFP in pGWB5	ERL2 genomic ΔKinase	pGWB5	KAN/HYG	KAN/HYG
pJSL73	FLS2ΔK in pENTR	FLS2ΔK cDNA no stop	pENTR	KAN	NA
pJSL75	35S:FLS2ΔK-GFP in pGWB5	FLS2ΔK cDNA no stop	pGWB5	KAN/HYG	KAN/HYG

Primer names	Sequences (5' to 3')	Purpose
EPFL9 1 XhoIf	CACCTCGAGATGAAGCATGAA	molecular cloning (pKUT608)
EPFL9 289 SpeI rc	ACTAGTTATCTATGACAAACAC	molecular cloning (pKUT608)
FLS2 1 (GW) F	CACCATGAAGTTACTCTCAAAGACCTTTTTG	molecular cloning (pJSL73)
FLS2 2625 rc	GATGTTGGCACTGTTGAATGAATCTGTTGC	molecular cloning (pJSL73)
FLS2 591 F	TGTAGCAGCTGGTAACCAT	Sequencing
eIF4A F	AGCCAGTGAGAATCTTGGTGAAGC	RT-PCR
eIF4A R	CTAGTACGGCAGAGCAAACACAGC	RT-PCR
STOMAGEN F	TGTAGTTCAAGCCTCAAGACCTC	RT-PCR
STOMAGEN R	ACTCGTTGTACGTACAAGTTGGT	RT-PCR
pER8 Term R	TCGAAACCGATGATACGGACG	RT-PCR
EPF1+207F	ATGCCGTCTTGTGATGGTTAG	RT-PCR
EPF1+315rc	TCAAGGGACAGGGTAGGACTT	RT-PCR
EPF2.1.cDNA.xhoI	CACCCTCGAGATGACGAAGTTTGTACGCAAGT	RT-PCR
EPF2.360.cDNA.ecoRI.rc2	CGGAATTCTAGCTCTAGATGGCACGTGATAG	RT-PCR